Acta Biomaterialia 54 (2017) 227–238

Contents lists available at ScienceDirect

Acta Biomaterialia

journal homepage: www.elsevier.com/locate/actabiomat

Full length article

Legumain-cleavable 4-arm poly(ethylene glycol)-doxorubicin conjugate for tumor specific delivery and release

Huicong Zhou [a,b,1], Huanjiao Sun [a,b,1], Shixian Lv [b], Dawei Zhang [b], Xuefei Zhang [a,*], Zhaohui Tang [b,*], Xuesi Chen [b]

[a] Key Laboratory of Environmentally Friendly Chemistry and Applications of Ministry of Education and Key Laboratory of Polymeric Materials & Application Technology of Hunan Province, Xiangtan University, Xiangtan 411105, PR China
[b] Key Laboratory of Polymer Ecomaterials, Changchun Institute of Applied Chemistry, Chinese Academy of Sciences, Changchun 130022, PR China

ARTICLE INFO

Article history:
Received 7 December 2016
Received in revised form 3 March 2017
Accepted 13 March 2017
Available online 15 March 2017

Keywords:
Legumain
PEG
Doxorubicin
Conjugate
Drug delivery

ABSTRACT

Traditional chemotherapy strategy exists undesirable toxic side-effects to normal tissues due to the low selectively to cancer cells of micromolecule cytotoxic drugs. One considered method to realizing the targeted delivery and increasing the specificity to tumor tissues of the cytotoxic drug is to transporting and discharging it through an environment-sensitive mechanism. In this study, a novel enzyme-sensitive polymer-doxorubicin conjugate was designed to delivery chemotherapeutic drug in a tumor-specific behavior and selectively activated in tumor tissue. Briefly, doxorubicin (DOX) was conjugated to carboxyl-terminated 4-arm poly(ethylene glycol) through a tetrapeptide linker, alanine-alanine-asparagine-leucine (AANL), which was one of the substrates of legumain, an asparaginyl endopeptidase that was found presented in plants, mammals and also highly expressed in human tumor tissues. Hereinafter, the polymer-DOX conjugate was termed as 4-arm PEG-AANL-DOX. Dynamic laser scattering (DLS) and transmission electron microscopy (TEM) measurements indicated that the 4-arm PEG-AANL-DOX could self-assemble into micelles in aqueous solution. Drug release and *in vitro* cytotoxicity studies revealed that the 4-arm PEG-AANL-DOX could be cleaved by legumain. *Ex vivo* DOX fluorescence imaging measurements demonstrated that the 4-arm PEG-AANL-DOX had an improved tumor-targeting delivery as compared with the free DOX·HCl. *In vivo* studies on nude mice bearing MDA-MB-435 tumors revealed that the 4-arm PEG-AANL-DOX had a comparable anticancer efficacy with the free DOX·HCl but without DOX-related toxicities to normal tissues as measured by body weight change and histological assessments, indicating that the 4-arm PEG-AANL-DOX had an improved therapeutic index for cancer therapy.

Statement of Significance

Herein we describe the construction of a novel tumor environment-sensitive delivery system through the instruction of a legumain-cleavable linkage to a polymer-DOX conjugate (4-arm PEG-AANL-DOX). This particular design strategy allows for polymer-DOX conjugates to be delivered in a tumor-specific manner and selectively activable in tumor microenvironment so that it can combine the advantages of tumor-specific delivery and tumor intracellular microenvironment-triggered release systems.

1. Introduction

Chemotherapy is among the most commonly used treatments for cancer therapy [1]. However, chemotherapeutic drugs aggressively kill both tumor and normal cells, thereby causing numerous undesirable severe side effects such as cardiotoxicity, renal toxicity, or the digestive tract toxicity and so on, these all are because of their non-specific distribution *in vivo*. In order to selectively eradicate tumor cells while minimizing toxicity to neighboring tissues, it is urgently needed to develop new chemotherapeutic agents which are delivered in a tumor-specific manner and selectively activated in tumor tissue.

* Corresponding authors.
E-mail addresses: zxf7515@163.com (X. Zhang), ztang@ciac.ac.cn (Z. Tang).
[1] These authors contributed equally to this work.

http://dx.doi.org/10.1016/j.actbio.2017.03.019
1742-7061/

Doxorubicin hydrochloride (DOX·HCl) is commonly used for the treatment of a variety of malignancy tumors, including sarcomas, leukemia and solid tumors [2]. However, the side effects of DOX·HCl, such as myelosuppression and cardiotoxicity, greatly impair its usages [3]. In order to enhance the therapeutic index of DOX·HCl, one frequently-used approach is to exert the tumor-specific delivery of DOX·HCl using nanocarriers which can primarily accumulate in tumor tissues *via* the "passive targeting" or "active targeting" after intravenous injection administration [4–16]. However, DOX·HCl must have access to target deoxyribonucleic acid (DNA) of tumor cells, not just at the tumor tissue lesion level. The "passive targeting" or "active targeting" can deliver DOX·HCl to tumor tissues, but the delivery of DOX·HCl to DNAs is still a challenge for nanomedicine. Generally speaking, DOX·HCl that is tightly encapsulated or conjugated in nanocarriers is difficult to liberate free active principle in tumor tissues. For example, PEGylated liposomal DOX (Doxil) is highly stable and releases active free DOX·HCl very slowly, hence its anticancer activity is only moderate [17]. To solve this problem, a number of tumor extracellular and intracellular microenvironment-triggered drug release systems were explored. Because the tumor extracellular and intracellular lysosomal environment is relatively acidic [18], acid-cleavable linkages, including hydrazone, maleyl and aconityl amide linkages, are widely used to conjugate DOX [19–23]. In addition, peptide linkers that are cleavable by tumor-associated endogenous proteases such as matrix metalloproteinases and cathepsin B, have attracted considerable attention [24–28].

Legumain/asparaginyl endopeptidase is a lysosomal/vascular cysteine protease and has a strict specificity for the hydrolysis of peptide bonds with asparagine or aspartic acid at the P1 position [29,30]. Legumain has an important role in the endosomal/lysosomal degradation system [31]. Under physiological conditions, legumain is mainly expressed in kidney [32,33]. Accumulating evidence shows that legumain is overexpressed on the surface of tumor-associated macrophages [34] and in a variety of solid tumors, such as carcinomas of the breast, colon, ovarian, prostate, central nervous system tumors, lymphoma and melanoma [35]. The level of legumain is positively correlated with the degree of malignancy. Overexpression of legumain is significant in tumors with high invasion and metastasis [36–42]. Because of the unique function and overexpression in many human tumors, legumain represents a promising target for the design of prodrugs and anticancer drug carriers [43]. Several legumain-cleavable small molecular anticancer drugs conjugates for tumor-specific active agent release have been reported [32,35,44–48], however, these small molecular conjugates could not deliver cytotoxic drugs in a tumor-specific manner.

Herein, we describe the construction of a novel tumor intracellular microenvironment-sensitive delivery system through the introduction of a legumain-cleavable tetrapeptide linkage to a polymer-DOX conjugate. This particular design strategy allows for polymer-DOX conjugates to be delivered in a tumor-specific manner and selectively activable in tumor intracellular microenvironment so that it can combine the advantages of tumor-specific delivery and tumor intracellular microenvironment-triggered release systems. For the proof of concept, a polymer-DOX conjugate (4-arm PEG-AANL-DOX) was prepared here by using AANL, a substrate of legumain [35], to link 4-arm PEG and DOX. The 4-arm PEG-AANL-DOX is expected to accumulate in a treated solid tumor *via* the enhanced permeability and retention (EPR) effect after injection *via* the tail vein, and specifically release active cytotoxic leucine-DOX molecules [49] at the tumor site where legumain is often highly upregulated. The 4-arm PEG-AANL-DOX was synthesized, characterized and evaluated *in vitro* and *in vivo* in detail.

2. Materials and methods

2.1. Materials

4-arm poly(ethylene glycol) (4-arm PEG-OH, M_n = 100 K) was purchased from the Pharmicell Co. Ltd, Korea and implemented as received. 3-(4,5-Dimethyl-thiazol-2-yl)-2,5-diphenyl tetrazolium bromide (MTT) and 4′, 6-diamidino-2-phenylindole dihydrochloride (DAPI) were purchased from Sigma–Aldrich. Doxorubicin hydrochloride (DOX·HCl) was purchased from Beijing Huafeng United Technology Corporation, China. Alanine-Alanine-Asparagine-Leucine (AANL) was custom-made by BAM Biotech Co., Ltd., Xiamen, China. Recombinant mouse legumain was purchased from Sino Biological Inc., Beijing, China. Benzotriazol-1-yl-oxytripyrrolidino-phosphonium hexafluorophosphate (PyBOP) and *N*-(3-dimethyl aminopropyl)-*N*′-ethylcarbodiimide hydrochloride (EDC·HCl) were purchased from Aladdin Industrial Corporation, Shanghai, China. *N*,*N*-Dimethylformamide (DMF), dichloromethane (DCM), pyridine (Py) and triethylamine (TEA) were dried by distillation over calcium hydride (CaH_2) before use. All the other reagents and solvents were purchased from Sinopharm Chemical Reagent Co. Ltd. and used without further purification.

2.2. Synthesis of 4-arm PEG-COOH

Succinic anhydride (4.00 g, 40.0 mmol) and 4-arm PEG-OH (20.0 g, 2.00 mmol) were dissolved in dry pyridine (50 mL), the solution was stirring at 25 °C for 48 h, then 250 mL DCM was added, after the pH of the reaction solution was tuned to 1.0 with aq. HCl (1 M), the mixture was then washed with saturated sodium chloride solution three times, dried with Na_2SO_4 and evaporated. The product was isolated by precipitation in excessive ice diethyl ether and dried under vacuum, yielding a white solid. ^{1}H NMR (400 MHz, $CDCl_3$, 298 K): δ (ppm) 4.26 (t, 2H, —OCH$_2$C*H*$_2$O(CO)—), 3.64 (s, 226H, —OC*H*$_2$C*H*$_2$O—), 3.41 (s, 2H, C(C*H*$_2$O—)), 2.64 (m, 4H, —(CO)C*H*$_2$C*H*$_2$(CO)—).

2.3. Synthesis of 4-arm PEG-NHS

4-arm PEG-COOH was activated with *N*-hydroxysuccinimide (NHS) in the presence of EDC·HCl at room temperature. Briefly, 4-arm PEG-COOH (15.0 g, 1.29 mmol), NHS (2.07 g, 18.0 mmol) and EDC·HCl (3.44 g, 18.0 mmol) were dissolved into dry DCM (150 mL). The solution was stirred overnight. Then the mixture was diluted with DCM, washed with saturated brine, dried over Na_2SO_4 and evaporated, precipitated in excessive ice diethyl ether and dried under vacuum. 4-arm PEG-NHS was obtained as a white solid. ^{1}H NMR (400 MHz, $CDCl_3$, 298 K): δ (ppm) 4.28 (t, 2H, —OCH$_2$C*H*$_2$O(CO)—), 3.64 (s, 225H, —OC*H*$_2$C*H*$_2$O—), 3.41 (s, 2H, C(C*H*$_2$O—)), 2.96 (t, 2H, —(CO)CH$_2$C*H*$_2$(CO)OSu), 2.84 (s, 4H, —C*H*$_2$-C*H*$_2$— from NHS), 2.78 (t, 2H, —(CO)C*H*$_2$CH$_2$(CO)OSu).

2.4. Synthesis of 4-arm PEG-AANL

The 4-arm PEG-AANL was prepared by the conjugation of 4-arm PEG-NHS to the N-terminus of peptide AANL. Briefly, the 4-arm PEG-NHS (2.00 g, 0.177 mmol), AANL (0.486 g, 1.20 mmol) and TEA (24.0 mg, 2.40 mmol) were dissolved in 20 mL of dry DMF. The conjugation reaction was carried out at 30 °C for 48 h. The solution was dialyzed with distilled water. The 4-arm PEG-AANL was obtained by lyophilization. ^{1}H NMR (400 MHz, trifluoroacetic acid-*d*, 298 K): δ (ppm) 4.97 (br, 1H, —C*H*< of Asn unit), 4.52 (br, 2H, —C*H*< of Ala unit), 4.42 (br, 1H, —C*H*< of Leu unit), 4.22 (br, 2H, —OCH$_2$C*H*$_2$O(CO)—), 3.70 (s, 227H, —OC*H*$_2$C*H*$_2$O—), 3.43 (s, 2H, C(C*H*$_2$O—)), 2.91 (m, 2H, —C*H*$_2$— of Asn unit), 2.66 (br, 2H,

—O(CO)CH_2CH_2(CO)—), 2.61 (br, 2H, —O(CO)CH_2CH_2(CO)—), 1.60 (br, 2H, —CH_2— of Leu unit), 1.30 (br, 6H, —CH_3 of Ala unit), 1.20 (br, 1H, —$CH(CH_3)_2$— of Leu unit), 0.77 (br, 6H, —CH_3 of Leu unit).

2.5. Synthesis of 4-arm PEG-AANL-DOX

To the stirring solution of 4-arm PEG-AANL (200 mg, 15.1 μmol) and DOX·HCl (69.6 mg, 120 μmol) in DMF (5 mL), TEA (62.5 mg, 618 μmol) and PyBOP (62.5 mg, 120 μmol) were added. The reaction mixture was stirred for 72 h in the dark, purified by dialysis against 0.01 M acetate buffer (pH = 5) in the dark. The 4-arm PEG-AANL-DOX was obtained after freeze-drying. ^{1}H NMR (400 MHz, trifluoroacetic acid-*d*, 298 K): δ (ppm) 7.85 (d, *H*-Ph), 7.67 (dd, *H*-Ph), 7.32 (d, *H*-Ph), 5.34 (br), 4.90 (m), 4.22 (br), 3.68 (s), 3.42 (s), 3.28 (d), 3.02–2.82 (m), 2.76 (s), 2.66 (br), 2.57 (br), 2.45 (d), 2.17 (dd), 1.60–1.37 (br), 1.29 (br), 1.22–1.11 (br), 0.73 (d).

2.6. Determination of DLC and DLE of the DOX conjugates

Drug loading content (DLC, wt.%) and drug loading efficiency (DLE, wt.%) of the 4-arm PEG-AANL-DOX were determined by UV–Vis spectrophotometry at 480 nm. DLC and DLE were calculated according to the following formulas:

$$\mathrm{DLC(wt.\%)} = (\text{weight of conjugated DOX} \cdot \mathrm{HCl}/\text{weight of conjugates}) \times 100\%$$

$$\mathrm{DLE(\%)} = (\text{weight of loaded DOX} \cdot \mathrm{HCl}/\text{weight of feeding DOX} \cdot \mathrm{HCl}) \times 100\%$$

2.7. Characterizations

^{1}H NMR spectra were carried on a Bruker AV 400 NMR spectrometer in chloroform-*d* ($CDCl_3$) or trifluoroacetic acid-*d* (CF_3-COOD). Dynamic laser scattering (DLS) and transmission electron microscopy (TEM) measurements were performed as our previous study [50,51]. Number-, weight-average molecular weights (M_n, M_w) and molecular weight distributions (polydispersity index, PDI = M_w/M_n) of the 4-arm PEG-NHS and 4-arm PEG-AANL were determined by gel permeation chromatography (GPC) using a system equipped with a Waters Ultrahydrogel Linear column, a 1515 HPLC pump and a 2414 Refractive Index detector. The eluent was phosphate buffer (PB, 0.2 M, pH 7.4) at flow rate of 1.0 mL/min at 25 °C. Monodispersed poly(ethylene glycol) standards were used to generate a calibration curve. GPC measurement of the 4-arm PEG-AANL-DOX was carried out on a GPC system equipped with a Waters 1515 HPLC pump, a series of linear Tskgel Super columns (AW3000 and AW5000), and a OPTILAB DSP interferometric refractometer. The eluent was DMF containing 0.01 M lithium bromide (LiBr) at a flow rate of 1.0 mL min^{-1} at 40 °C. Monodispersed polystyrene standards with different molecular weights were used to generate the calibration curve. Unconjugated DOX in the polymer-DOX conjugates was determined using a Waters 1525 Binary HPLC pump with the detector set at 480 nm using acetonitrile and water (4:1, v/v) as a mobile phase.

2.8. Cell cultures

MDA-MB-435 and 4T1 cells were grown at 37 °C in a 5% CO_2 atmosphere in Dulbecco's Modified Eagle Medium (DMEM) with 10% fetal bovine serum, penicillin (50 U mL^{-1}) and streptomycin (50 U mL^{-1}).

2.9. Confocal laser scanning microscopy observation

MDA-MB-435 cells were seeded in 6-well plates with a density of 1.0×10^5 cells per well in 2 mL of DMEM and incubated for 24 h, then the cells were treated with free DOX·HCl or 4-arm PEG-AANL-DOX. After 12 or 24 h incubation, the medium was removed, the cells were washed three times with phosphate buffered saline (PBS, pH = 7.4) and fixed with 4% formaldehyde for 10 min at

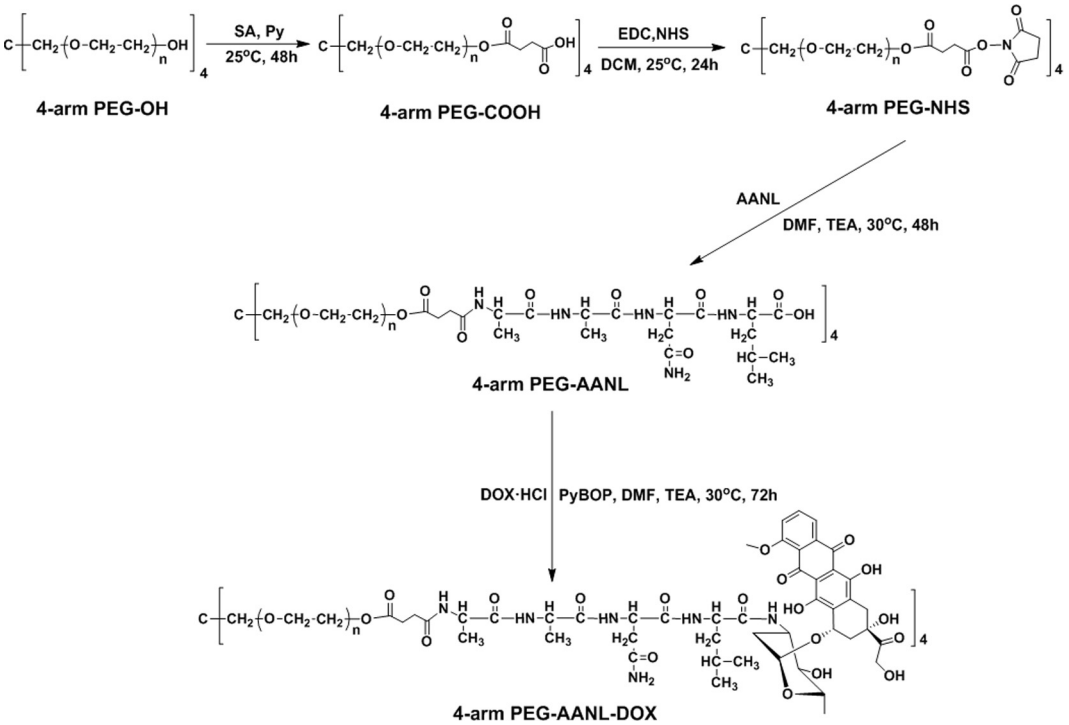

Scheme 1. Preparation of 4-arm PEG-DOX and 4-arm PEG-AANL-DOX.

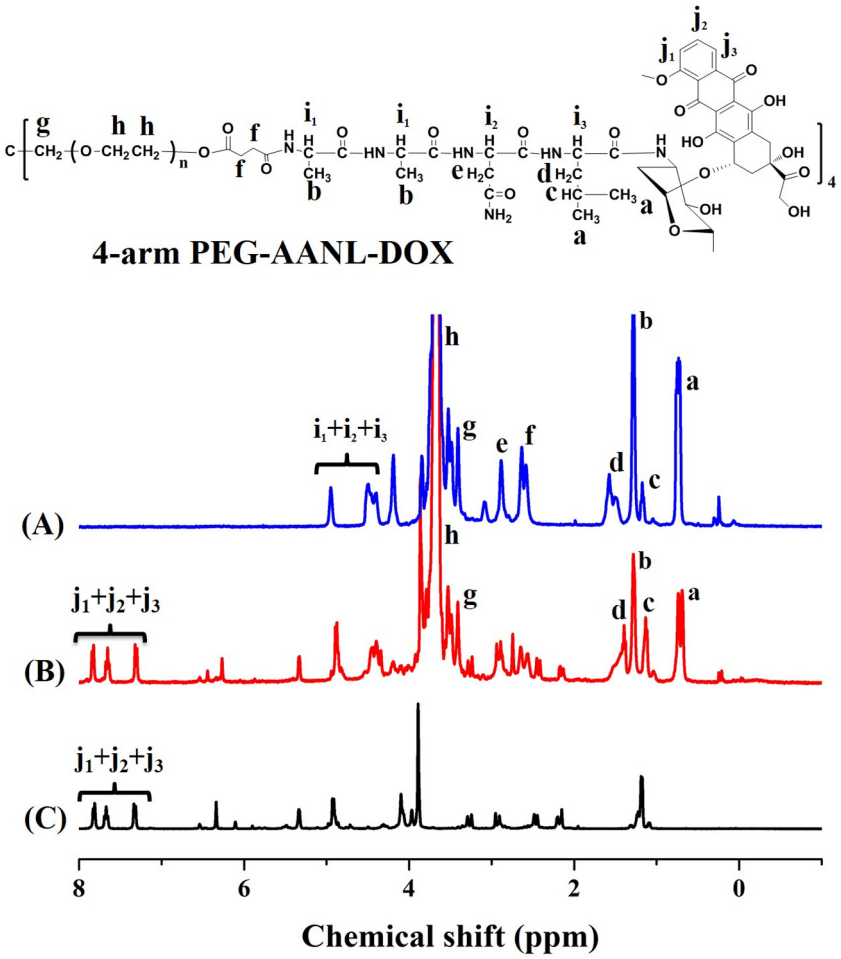

Fig. 1. ^{1}H NMR spectra of 4-arm PEG-AANL (A) and 4-arm PEG-AANL-DOX (B) and DOX·HCl (C) in CF_3COOD.

37 °C. The cell nucleus were stained with 0.1% DAPI for 10 min in the dark and washed with PBS three times. The treated cells were visualized with a Carl Zeiss LSM 780 confocal laser microscope.

2.10. Drug release in the presence/absence of legumain

To a 50 μL citric acid buffer (pH 4.5, containing 50 mM citric acid, 1 mM DTT, 1 mM EDTA) with or without recombinant mouse legumain (10 μg), 4-arm PEG-AANL-DOX aqueous solution (1.0 mg/mL, 50 μL) was added. The mixture was incubated at 37 °C and aliquots (10 μL) were removed at various time points (12, 24, 48 and 72 h). The aliquots (10 μL) were diluted with methanol (1.0 mL) and centrifuged at 9600*g* for 10 min at room temperature. The supernatant was collected and diluted to 3.0 mL with deionized water. The obtained solution was moved to an ultrafiltration centrifuge tube (MWCO 3500 Da) and

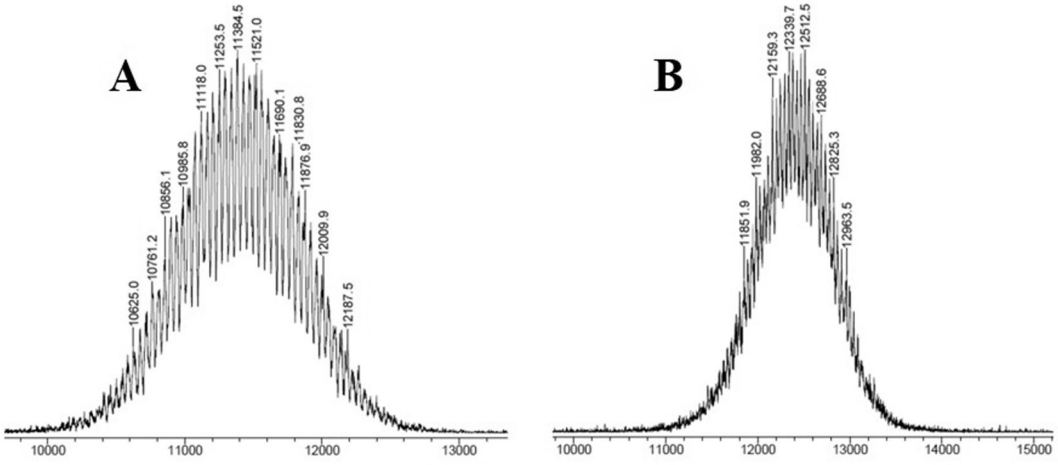

Fig. 2. MALDI-TOF MS spectra of 4-arm PEG-NHS (A) and 4-arm PEG-AANL (B).

centrifuged at 1500*g* for 30 min. The ultrafiltrate was collected. The amount of cleaved 4-arm PEG-AANL-DOX in the ultrafiltrate was determined using fluorescence spectroscopy (Excitation and emission wavelengths for doxorubicin, were set at 480 and 590 nm, respectively). Data are presented as mean ± STD ($n = 3$).

2.11. In vitro cytotoxicity assays

The *in vitro* cytotoxicity of free DOX·HCl and 4-arm PEG-AANL-DOX were evaluated by MTT assay in the MDA-MB-435 and 4T1 cell lines. Cells were seeded in 96-well plates with 1.0×10^5 cells per well in 100 μL DMEM for 24 h. Then culture medium was removed, fresh DMEM containing the free DOX·HCl or 4-arm PEG-AANL-DOX was added in different concentrations. After another 48 h or 72 h incubation, cell viability was analyzed using MTT assay with a Bio-Rad 680 microplate reader at a wavelength of 490 nm. The relative cell viability was determined by comparing the absorbance at 490 nm with control wells containing only cell culture medium. Data are presented as mean ± STD ($n = 3$).

2.12. Animals

Female Balb/C nude mice (6–8 weeks old) were purchased from Beijing Huafukang Biological Technology Co. Ltd. (HFK Bioscience, Beijing). All experimental animals received well care and approved by the Animal Care and Use Committee of Jilin University.

2.13. Ex vivo DOX fluorescence imaging

Free DOX·HCl and 4-arm PEG-AANL-DOX (5 mg/kg on a DOX·HCl basis) were injected into nude mice bearing MDA-MB-435 tumor *via* tail vein. The mice were sacrificed 2 or 24 h after injection. The tumors and visceral organs (heart, kidney, liver, lung and spleen) were excised, followed by washing the surface with physiological saline three times. The *ex vivo* imaging of DOX fluorescence was carried out on a Maestro *in vivo* Imaging System from Cambridge Research & Instrumentation, Inc., USA. The resulting data were analyzed using commercial software (Maestro software version 2.4, CRi).

2.14. In vivo anti-tumor efficacy study

A human cancer xenograft tumor model was built by the subcutaneous injection of MDA-MB-435 cells (1.5×10^6) into the right mammary fat pad of each mouse. When the tumor volume was about 50 mm^3, the mice were divided into 4 groups ($n = 6$) and then treated with PBS, DOX·HCl (5 mg/kg), 4-arm PEG-AANL-DOX (5 mg/kg on a DOX·HCl basis) or 4-arm PEG-AANL-DOX (15 mg/kg on a DOX·HCl basis) by tail intravenous injection six times on days 0, 4, 8, 12, 16 and 20. Tumor size and body weight were measured every two days to evaluate the antitumor activity and systemic toxicity. Tumor volume was measured using a Vernier caliper. Tumor volume = $a \times b^2/2$, where a is the length and b is the width of the tumors.

2.15. Hematoxylin-eosin staining

At day 36 of the treatment, all MDA-MB-435 tumor-bearing mice were sacrificed. Tumors and major organs were excised and fixed in 4% PBS buffered paraformaldehyde overnight, and then embedded in paraffin. The paraffin embedded tumors and organs were cut at 5 mm thickness, and stained with hematoxylin and eosin (H&E) to assess histological alterations by microscope (Nikon TE2000U).

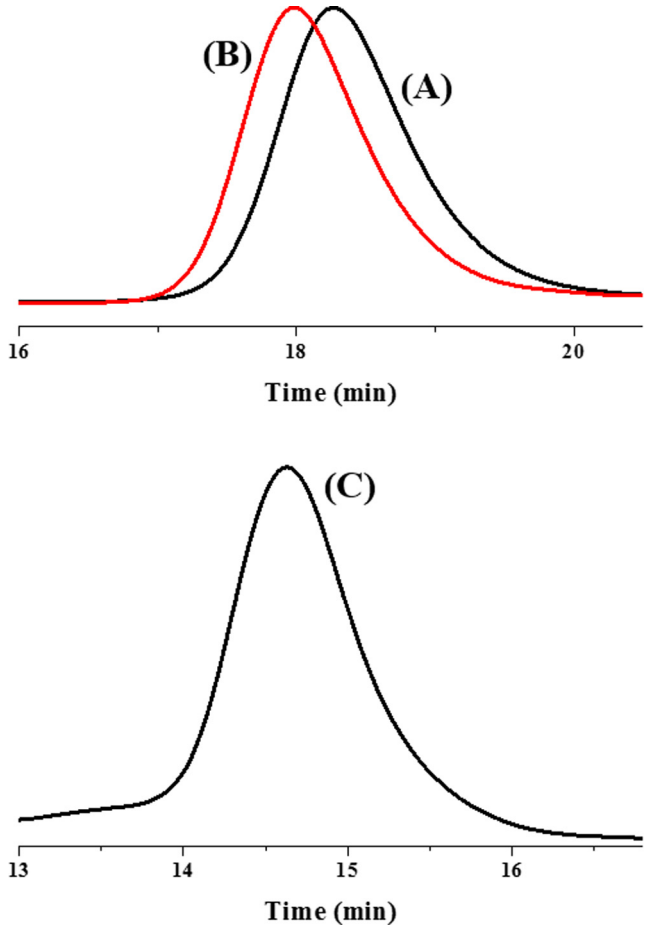

Fig. 3. GPC traces of 4-arm PEG-NHS (A), 4-arm PEG-AANL (B) and 4-arm PEG-AANL-DOX (C).

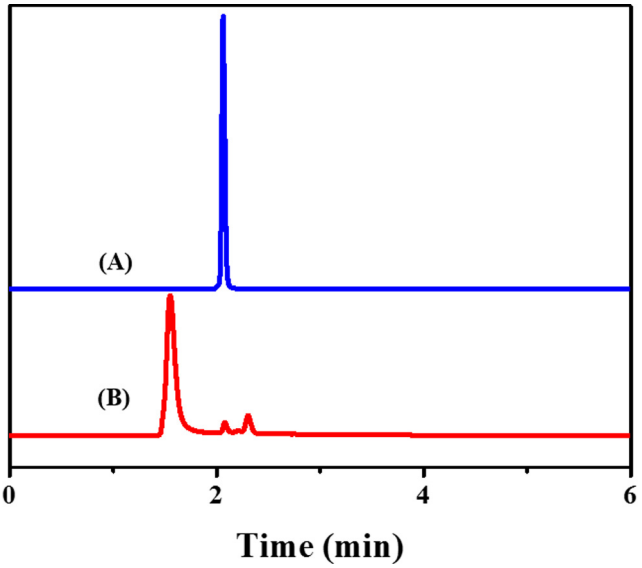

Fig. 4. The HPLC curves of DOX·HCl (A) and 4-arm PEG-AANL-DOX (B).

2.16. Statistical analysis

Data are expressed as the mean ± STD. Statistical significance was determined using the Student's *t*-test. $p < 0.05$ was considered statistically significant, and $p < 0.01$ was considered highly significant.

3. Results and discussion

3.1. Synthesis and characterization of polymer–DOX conjugate

As shown in Scheme 1, 4-arm PEG-AANL-DOX was prepared in 4 steps. Firstly, 4-arm PEG-COOH was prepared by the reaction of 4-arm PEG-OH with succinic anhydride. Secondly, 4-arm PEG-NHS was obtained by the reaction of 4-arm PEG-COOH with N-hydroxysuccinimide. Thirdly, 4-arm PEG-AANL was synthesized by the conjugation of the AANL to the 4-arm PEG-NHS. Finally, the 4-arm PEG-AANL-DOX was made by the amide-forming reaction of the 4-arm PEG-AANL with DOX·HCl using PyBOP as condensation reagent at the presence of TEA.

The ^{1}H NMR spectra of the DOX·HCl, 4-arm PEG-AANL and 4-arm PEG-AANL-DOX are shown in Fig. 1. For the 4-arm PEG-AANL, the signals at δ 3.43, 2.66–2.61 and 0.77 ppm were assigned to the protons of C(CH_2O—) (g), —O(CO)CH_2CH_2(CO)— (f) and —CH_3 of Leu unit (a), respectively. The intensity ratio of signals at δ 3.43, 2.66–2.61 and 0.77 ppm was 1:2:3 (Fig. 1A), suggesting that all the arms of the 4-arm PEG were connected to —(CO)CH_2CH_2(CO)-AANL groups in the obtained 4-arm PEG-AANL. MALDI-TOF MS analysis (Fig. 2) showed M_n (4-arm PEG-AANL) > M_n (4-arm PEG-NHS). After conjugation of DOX, the 4-arm PEG-AANL-DOX showed peaks (j_1 + j_2 + j_3) in the range of δ 7.28–7.93 ppm (*H*-Ph in DOX) in the ^{1}H NMR spectrum (Fig. 1B) as comparing with the 4-arm PEG-AANL, indicating that DOX was successfully conjugated to the 4-arm PEG-AANL. GPC analyses (Fig. 3) revealed that the 4-arm PEG-NHS, 4-arm PEG-AANL and 4-arm PEG-AANL-DOX had a narrow, unimodal molecular weight distribution (PDI = 1.29, 1.27 and 1.07, respectively). These data confirmed that the 4-arm PEG-AANL-DOX was prepared successfully.

HPLC curves of DOX·HCl and 4-arm PEG-AANL-DOX were shown in Fig. 4. The peak of DOX·HCl at 2.07 min almost disappeared in the spectrum of the 4-arm PEG-AANL-DOX, indicating that the polymer-DOX conjugate had a high purity. According to the HPLC results, only 2.7% of DOX existed in the form of free drug in the obtained 4-arm PEG-AANL-DOX, which further confirmed that polymer-DOX conjugate was prepared successfully.

Considering that multi-arm PEG could bring relatively high DLC, the 4-arm PEG-OH was selected for conjugate preparation. The DLC and DLE of the 4-arm PEG-AANL-DOX were determined by UV–Vis spectrophotometry. The DLC and DLE for the 4-arm PEG-AANL-DOX were 14.9 wt.% and 89.3% (Table 1), respectively.

For comparison, a control drug conjugate without legumain cleavable linker (4-arm PEG-DOX) was prepared by the reaction of 4-arm PEG-NHS with DOX·HCl in DMF at the presence of TEA (Please see Supplementary Materials). The ^{1}H NMR spectrum of the obtained 4-arm PEG-DOX in CF_3COOD was shown in Fig. S1. Clear signals from DOX and PEG moieties could be found in the spectrum. HPLC measurement (Fig. S2) showed that only 2.3% of DOX existed in the form of free drug in the obtained 4-arm PEG-DOX sample, which further confirmed that the 4-arm PEG-DOX was prepared successfully. The DLC of the 4-arm PEG-DOX determined by UV–Vis spectrophotometry were 13.5 wt.%, which is close to that of the 4-arm PEG-AANL-DOX.

3.2. Self-assembly of polymer–DOX conjugates

Amphiphilic polymers that have hydrophilic and hydrophobic domains can form micelles by self-assembling in aqueous solution. Due to the hydrophilicity of PEG segments, 4-arm PEG-AANL-DOX can be directly dissolved in water to obtain micelles [7].

Table 1
Characterizations of DOX·HCl and 4-arm PEG-AANL-DOX.

Polymer-DOX conjugates	DLC%[a]	DLE%[a]	IC_{50} (μg mL^{-1})[b]			
			MDA-MB-435		4T1	
			48 h	72 h	48 h	72 h
DOX·HCl	/	/	1.20	0.56	0.22	0.26
4-arm PEG-AANL-DOX	14.9	89.3	5.37	2.82	> 10	> 10

[a] Determined by UV–Vis spectrophotometry.
[b] Determined by MTT.

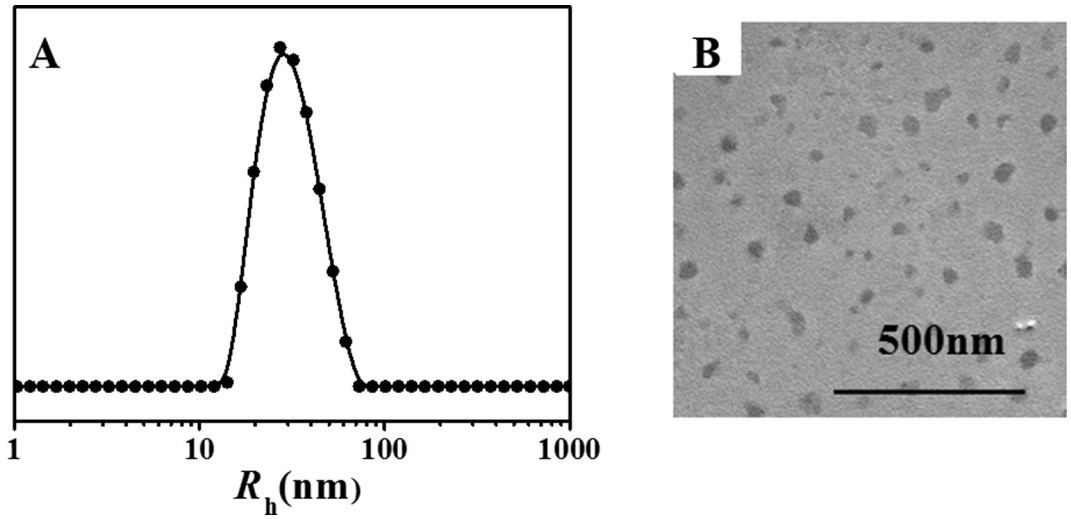

Fig. 5. DLS size distribution (A) and typical TEM image (B) of 4-arm PEG-AANL-DOX micelles.

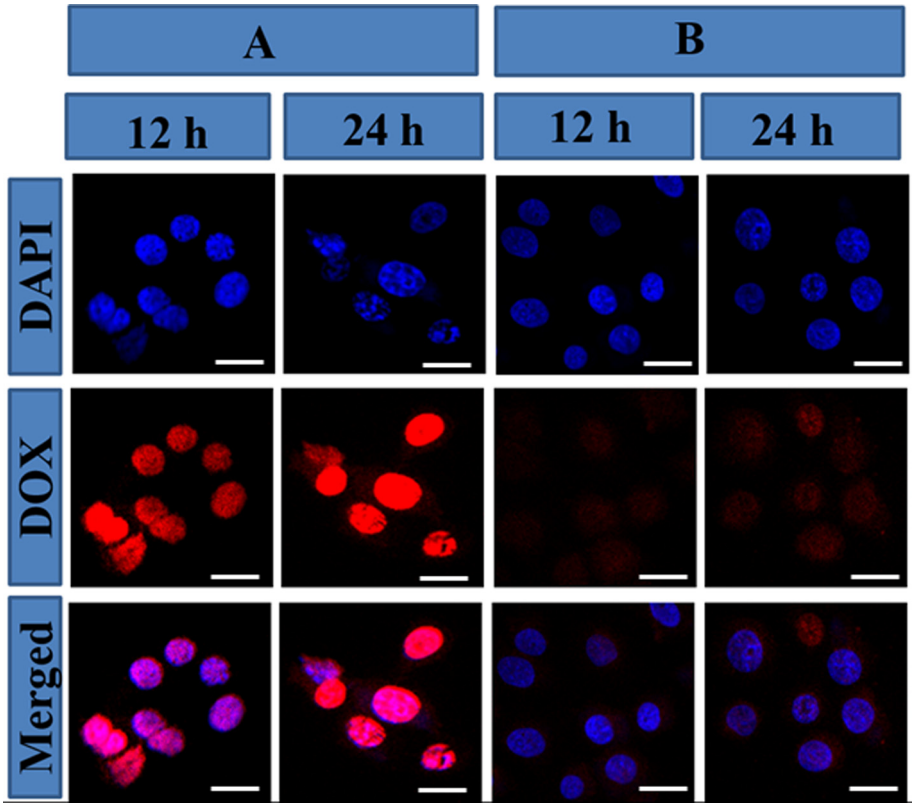

Fig. 6. CLSM images of MDA-MB-435 cells (scale bar = 20 μm) after incubation with free DOX·HCl (A) and 4-arm PEG-AANL-DOX (B) in identical concentration on the basis of net DOX·HCl for 12 and 24 h.

The hydrodynamic sizes of the polymer–DOX conjugate micelles were determined by DLS measurements. As shown in Fig. 5A, 4-arm PEG-AANL-DOX micelles had a narrow size distribution. The hydrodynamic radius (R_h) of the 4-arm PEG-AANL-DOX micelles was 32 ± 11 nm. TEM micrograph showed that the 4-arm PEG-AANL-DOX micelles had an average radius around 23 ± 5 nm (Fig. 5B). The smaller values from TEM observations could be explained by the dehydration of the micelles in the sample preparation process [52]. The size of the 4-arm PEG-AANL-DOX micelles will bring great advantages for solid tumor targeting delivery *via* EPR effect because they are in the ideal range to avoid the filtration by kidney (R_h > 10 nm) and sequestration by spleen and liver (R_h < 50 - nm) [53].

3.3. Intracellular drug delivery

In order to evaluate the cellular uptake and intracellular release of drug, 4-arm PEG-AANL-DOX micelles and free DOX·HCl were incubated with MDA-MB-435 cells for 12 h or 24 h at 37 °C. CLSM was used for the observation of the cells (Fig. 6). The cellular nuclei were stained with DAPI (blue) for subcellular observation. Red fluorescence imaging was employed for the visualization of the released active small molecular agents. For the free DOX·HCl-treated cells (A), strong DOX fluorescence was found to be primarily located in the nuclei because free DOX·HCl could pass quickly through the MDA-MB-435 cell membrane to the cytosol and be rapidly transported to the nuclei and bound to the DNA [54]. For the cells treated with 4-arm PEG-AANL-DOX (B), the DOX fluorescence was located in both cytoplasm and nuclei and much weaker than that of free DOX·HCl-treated cells. These could be explained as follows. The 4-arm PEG-AANL-DOX was taken up by the cells through endocytosis and trapped in subcellular compartments (endosomes and lysosomes). Subsequently, the subcellular environment induced the cleavage of bonds and the release of free DOX. Therefore, the doxorubicin fluorescence of 4-arm PEG-AANL-DOX micelles-treated cells was weaker than that of free DOX·HCl-treated cells and distributed in both the cytoplasm and nuclei. The 4-arm PEG-AANL-DOX-treated cells showed stronger DOX fluorescence intensity in nuclei than those treated with

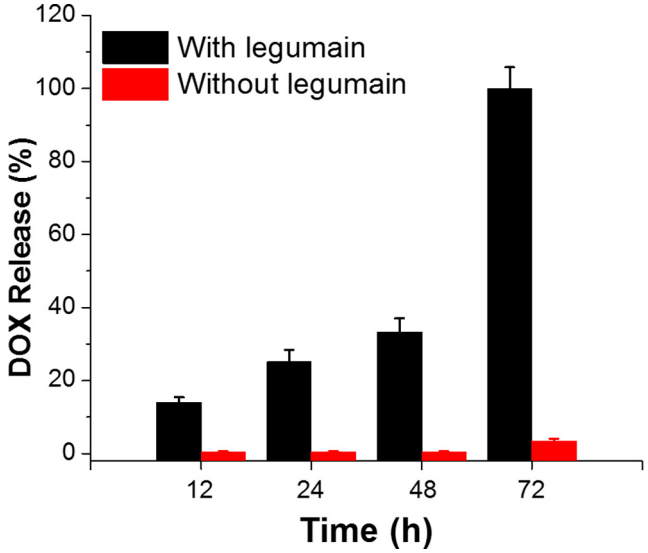

Fig. 7. Drug release from the 4-arm PEG-AANL-DOX in the citric acid buffer in the presence/absence of legumain. Data were presented as the mean ± STD (n = 3).

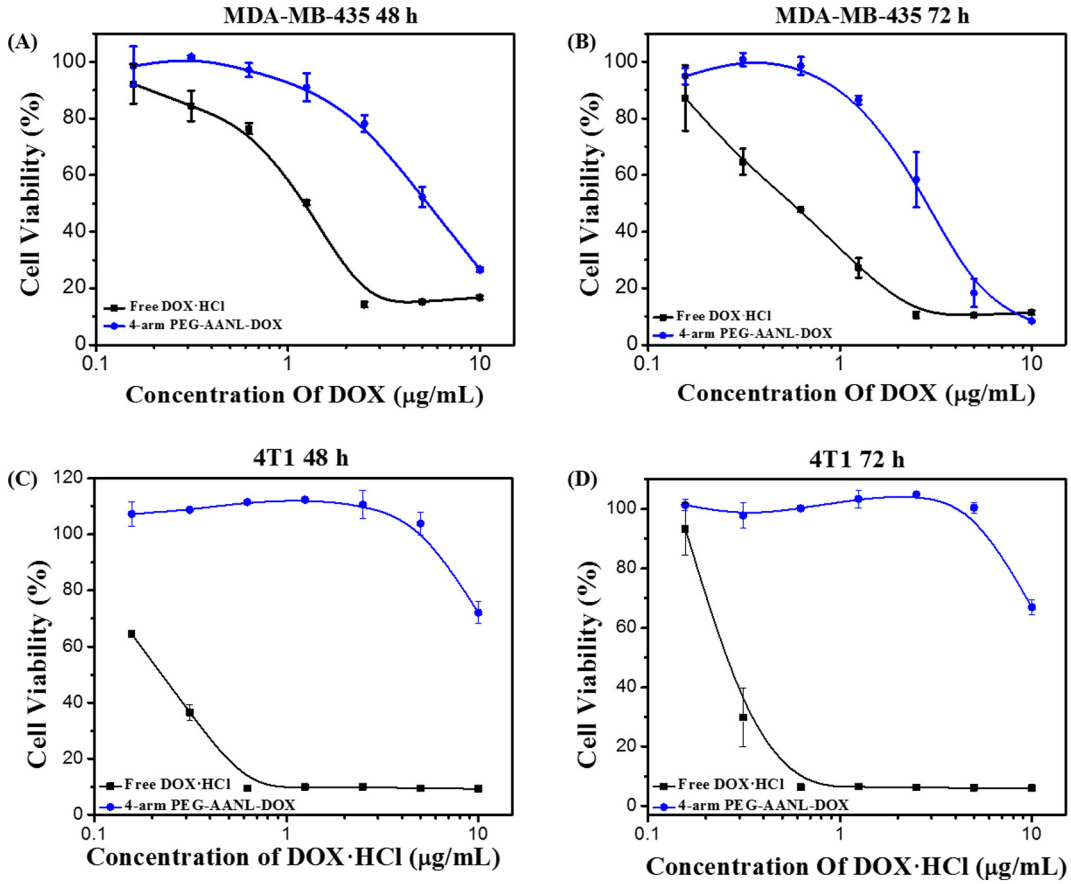

Fig. 8. *In vitro* cell viabilities of legumain-overexpressed MDA-MB-435 and legumain-lowexpressed 4T1 cells incubated with free DOX·HCl, 4-arm PEG-DOX or 4-arm PEG-AANL-DOX for 48 h (A) and 72 h (B). DOX·HCl concentration is based on net DOX·HCl. Data were presented as the mean ± STD (n = 3).

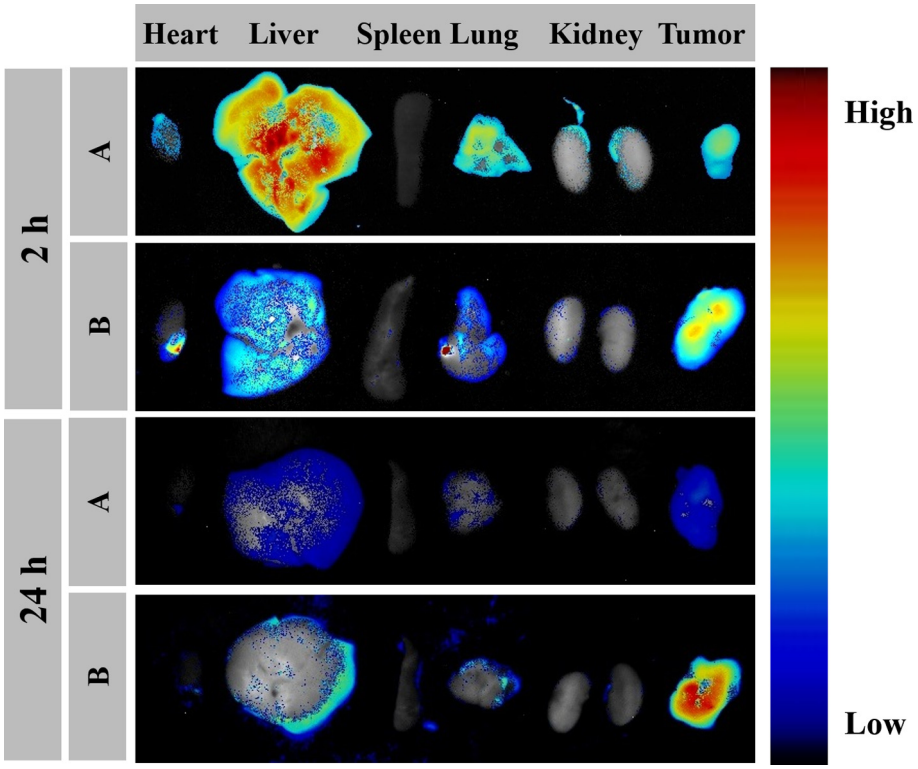

Fig. 9. *Ex vivo* DOX fluorescence images showing the drug biodistribution of (A) free DOX·HCl and (B) 4-arm PEG-AANL-DOX in nude mice bearing MDA-MB-435 tumor at 2 and 24 h postinjection. Dosage for all the mice: 5 mg/kg on the basis of net DOX·HCl.

4-arm PEG-DOX, indicating an increased rate in DOX release, which could be attributed to the legumain-cleavable AANL linkage in the 4-arm PEG-AANL-DOX (Fig. S3).

3.4. Drug release in the presence/absence of legumain

To investigate the influence of legumain on the polymer-DOX conjugate, drug release from the 4-arm PEG-AANL-DOX in the citric acid buffer was carried out in the presence/absence of a catalytic amount of legumain. As shown in the Fig. 7, a complete release of small molecular drug from the 4-arm PEG-AANL-DOX was observed after 72 h incubation with the legumain protease. In contrast, less than 4% of DOX was released in the absence of legumain protease. This indicated that the drug release rate from the 4-arm PEG-AANL-DOX was much higher in the presence of legumain than that in the absence of legumain, suggesting the 4-arm PEG-AANL-DOX was legumain-activable. Because the released leucine-DOX has higher maximum tolerated dose and efficacy than free DOX·HCl [49], it would make sense to compare the anticancer activity of 4-arm PEG-AANL-DOX and free DOX·HCl *in vitro* and *in vivo*.

3.5. In vitro cytotoxicity study

To further confirm that the 4-arm PEG-AANL-DOX is activable in the presence of legumain, the relative cytotoxicities of free DOX·HCl and 4-arm PEG-AANL-DOX were evaluated against MDA-MB-435 and 4T1 cancer cells for 48 and 72 h using MTT assay. The MDA-MB-435 and 4T1 cell lines were selected in this study because the MDA-MB-435 cells expressed active legumain in high level and the 4T1 cells *in vitro* had only weak expression of active legumain [45,46]. The MTT results are presented in Fig. 8 and Table 1. The IC_{50} (48 h) of free drug (DOX·HCl) against MDA-MB-435 cells (1.20 μg/mL) was much higher than that of 4T1 cells (0.22 μg/mL). In contrast, the IC_{50} (48 h) of the 4-arm PEG-AANL-DOX against MDA-MB-435 cells (5.37 μg/mL) was much smaller than that of and 4T1 cells (>10 μg/mL). The IC_{50} (48 h) ratio of DOX·HCl/4-arm PEG-AANL-DOX was 4.5 for the legumain-overexpressed MDA-MB-435 cells, by contrast, the IC_{50} (48 h) ratio increased to over 45.5 for the legumain-lowexpressed 4T1 cells. Similar phenomenon was also observed for 72 h incubation time. These indicated that cytotoxic DOX could be efficiently liberated from the 4-arm PEG-AANL-DOX in the legumain-overexpressed MDA-MB-435 cells, but not in the legumain-lowexpressed 4T1 cells *in vitro*. The IC_{50} (48 h) and IC_{50} (72 h) of the 4-arm PEG-DOX towards legumain-overexpressed MDA-MB-435 cells were much higher than 10 μg/mL (Fig. S4). This further indicated that the legumain-cleavable AANL linkage in the 4-arm PEG-AANL-DOX was important for increased activity.

3.6. Ex vivo DOX fluorescence imaging

In order to investigate the tumor targeting ability of free DOX·HCl and 4-arm PEG-AANL-DOX, the *ex vivo* imaging of the isolated tumors and visceral organs of MDA-MB-435 tumor bearing Balb/C nude mice at 2 and 24 h post-injection was carried out (Fig. 9). At 2 h, liver displayed strong DOX fluorescence for all the formulations, revealing that DOX·HCl was mainly captured and metabolized by the liver. As compared with the free DOX·HCl group, stronger fluorescence in tumor was observed in the group of 4-arm PEG-AANL-DOX, indicating that the 4-arm PEG-AANL-DOX could alter the biodistribution of the chemotherapeutic drug. At 24 h, fluorescence in liver greatly faded in the *ex vivo* imaging for all the formulations, and meanwhile tumor showed slightly weaker DOX fluorescence for the free DOX·HCl. It is noteworthy that a much stronger DOX fluorescence was observed in tumors treated with the 4-arm PEG-AANL-DOX compared to that of free DOX·HCl, indicating less reticuloendothelial system sequestration and more tumor accumulation for the polymer-DOX conjugates than free DOX·HCl.

3.7. In vivo antitumor efficacy

In order to further examine the *in vivo* tumor inhibitory activities of different DOX formulations, female Balb/C nude mice bearing MDA-MB-435 tumors were divided into 4 groups and injected six times at 4 d intervals with PBS, free DOX·HCl (5 mg/kg), or 4-arm PEG-AANL-DOX (5 and 15 mg/kg eq.) *via* tail vein. As shown in Fig. 10A, all DOX formulations showed some efficacy in inhibiting tumor growth as compared with the PBS-treated group. At the end of the experiment, the reduction in tumor volume in mice receiving free DOX·HCl (5 mg/kg) and 4-arm PEG-AANL-DOX (5 mg/kg eq.) were 71.6% and 56.6%, respectively. This indicated that the tumor inhibition ability of the 4-arm PEG-AANL-DOX was slightly weaker than that of free DOX·HCl at equal dosage. The inhibitory effect of the 4-arm PEG-AANL-DOX could be further improved by increasing the dosage to 15 mg/kg eq., which showed a 77.7% reduction in tumor volume at the end of 36 days. This was slightly higher than that of free DOX·HCl (5 mg/kg) group. The reduction in tumor volume in mice receiving 4-arm PEG-DOX (5 mg/kg eq.) was 35.2% (Fig. S5). This was significantly lower than

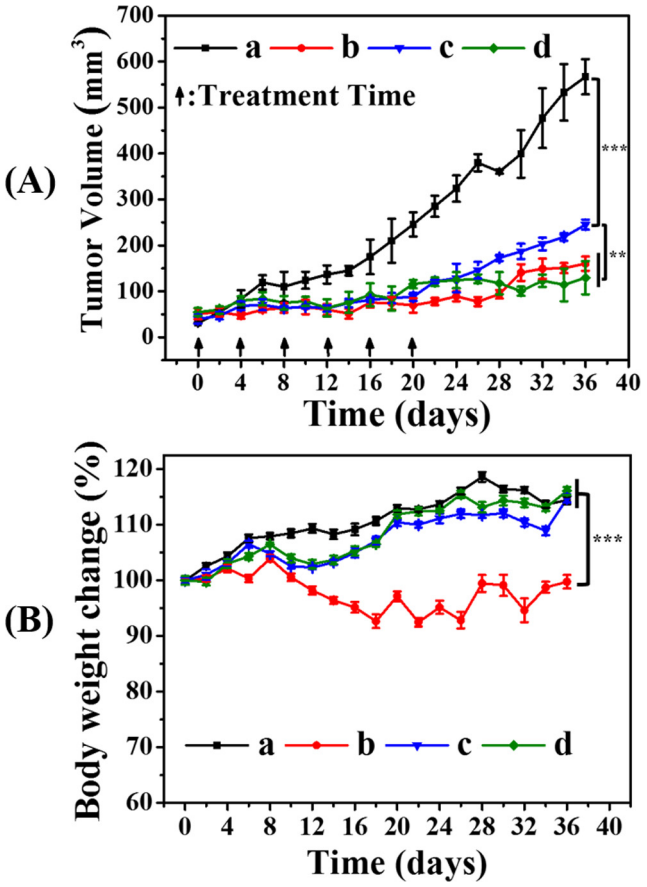

Fig. 10. *In vivo* anti-tumor efficacies of various DOX formulations in the MDA-MB-435 tumor bearing Balb/C nude mice model. (A) Tumor volume growth curve. (B) Body weight changes of tumor-bearing mice with the time. Tumor sizes and body weight changes were measured every 2 days. The mice were treated on days 0, 4, 8, 12, 16 and 20 with PBS (a), DOX·HCl (5 mg/kg) (b), 4-Arm PEG-AANL-DOX (5 mg/kg eq.) (c) or 4-arm PEG-AANL-DOX (15 mg/kg eq.) (d). Dosage for all the groups is based on net DOX·HCl. The data are shown as mean ± STD ($n = 6$). $^{**}p < 0.01$, $^{***}p < 0.001$.

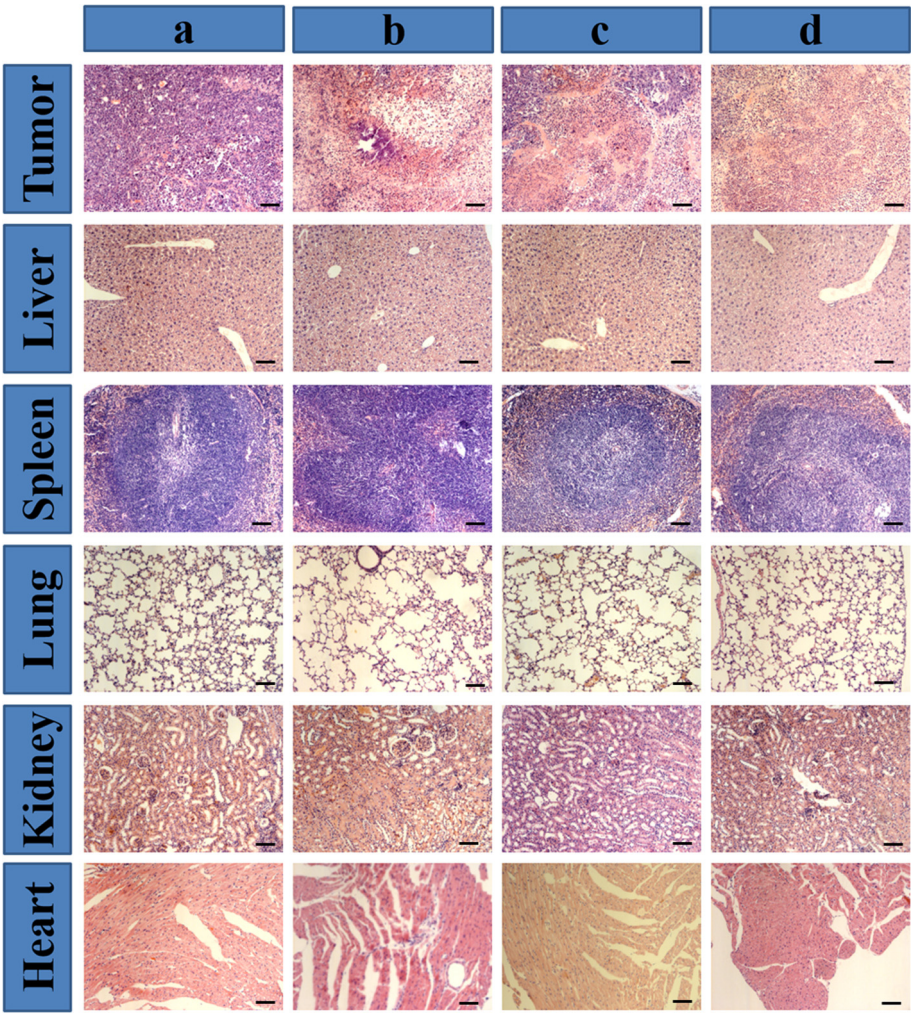

Fig. 11. H&E analyses of tumors and major organs of MDA-MB-435 tumor bearing Balb/C nude mice (scale bar = 200 μm): (a) PBS; (b) free DOX·HCl (5 mg/kg); (c) 4-arm PEG-AANL-DOX (5 mg/kg eq.); (d) 4-arm PEG-AANL-DOX (15 mg/kg eq.). Dosage for all the groups is based on net DOX·HCl.

that of PEG-AANL-DOX (5 mg/kg eq.), indicating that the tumor inhibition ability of 4-arm PEG-AANL-DOX is much higher than that of 4-arm PEG-DOX at equal dose, further confirming that the legumain-cleavable AANL linkage in the 4-arm PEG-AANL-DOX was important for increased anticancer activity. All the mice were alive during the whole experimental period, body weight change could clearly reflect drug-related systemic toxicity. As shown in Fig. 10B, a significantly body weight loss was observed in the free DOX·HCl (5 mg/kg) treatment group (5.4% body weight loss), while the 4-arm PEG-AANL-DOX treatment groups did not show any body weight loss during the 36 days observation period, even if the dosage was three folds of the free DOX·HCl. These results demonstrated that the 4-arm PEG-AANL-DOX possessed enhanced antitumor efficacy and lower drug related toxicity over free DOX·HCl by using a proper dosage, that is to say, the 4-arm PEG-AANL-DOX have an improved therapeutic index than the free DOX·HCl, indicating that the legumain-cleavable polymer-DOX conjugate is promising in cancer therapy.

3.8. Histopathology evaluation

To further evaluate the anticancer activity of various DOX formulations, tumors and visceral organs were dissected from mice on day 36 and sectioned for H&E analyses and the results were shown in Fig. 11. A number of cells with large nuclei, a spherical or spindle shape, or more chromatin and binucleolates were observed in the tumor tissue from PBS-treated group, revealing a rapid tumor growth. In contrast, significant tumor tissue necrosis was seen in all the DOX formulation-treated groups. The tendency of necrotic level was (d) 4-arm PEG-AANL-DOX (15 mg/ kg eq.) > (b) free DOX·HCl (5 mg/kg) > (c) 4-arm PEG-AANL-DOX (5 mg/kg eq.) > (a) PBS, which was consistent with the results of *in vivo* antitumor efficacy study. Treatments with the free DOX·HCl and 4-arm PEG-AANL-DOX have not caused significant morphological changes in liver, spleen, lung and kidney compared to the PBS group. However, it is worth noting that the group treated with free DOX·HCl (group b) had noticeable signals of heart damage, with critical pathological changes and muscle fibers necrosis in cardiac tissues. In contrast, treatments by the 4-arm PEG-AANL-DOX (group c and d) obviously reduced the blight of heart, indicating reduced cardiotoxicity. This explained why the 4-arm PEG-AANL-DOX exhibited lower systemic toxicity than the free DOX·HCl in the *in vivo* antitumor efficacy study. Based on the results received from the tumor volume growth curve, body weight change and H&E staining, a 4-arm PEG-AANL-DOX with a higher therapeutic index than the free DOX·HCl was achieved.

4. Conclusions

In summary, a novel legumain-cleavable polymer-DOX conjugate, 4-arm PEG-AANL-DOX, was designed and prepared *via* a typical amide-forming condensation reaction here. The 4-arm PEG-AANL-DOX could be delivered in a tumor-specific manner and selectively activable in legumain overexpressed tumor intracellular microenvironment. The 4-arm PEG-AANL-DOX showed high antitumor efficacy without systemic toxicity compared to free DOX·HCl. Thus, the legumain-cleavable 4-arm PEG-AANL-DOX is a promising drug delivery system for cancer therapy.

Acknowledgments

This research was financially supported by National Natural Science Foundation of China (Projects 51673189, 51473029, 51233004, 51473141, 51273169, 51528303 and 51403204) and the Chinese Academy of Sciences Youth Innovation Promotion Association.

Appendix A. Supplementary data

Supplementary data associated with this article can be found, in the online version, at http://dx.doi.org/10.1016/j.actbio.2017.03.019.

References

[1] E. Blanco, A. Hsiao, A.P. Mann, M.G. Landry, F. Meric-Bernstam, M. Ferrari, Nanomedicine in cancer therapy: innovative trends and prospects, Cancer Sci. 102 (7) (2011) 1247–1252.
[2] O. Tacar, P. Sriamornsak, C.R. Dass, Doxorubicin: an update on anticancer molecular action, toxicity and novel drug delivery systems, J. Pharm. Pharmacol. 65 (2) (2013) 157–170.
[3] Q. Li, S. Lv, Z. Tang, M. Liu, D. Zhang, Y. Yang, X. Chen, A co-delivery system based on paclitaxel grafted mPEG-b-PLG loaded with doxorubicin: preparation, in vitro and in vivo evaluation, Int. J. Pharm. 471 (1–2) (2014) 412–420.
[4] Y. Matsumura, H. Maeda, A new concept for macromolecular therapeutics in cancer chemotherapy: mechanism of tumoritropic accumulation of proteins and the antitumor agent smancs, Cancer Res. 46 (12 (Part 1)) (1986) 6387–6392.
[5] H. Maeda, K. Tsukigawa, J. Fang, A retrospective 30 years after discovery of the enhanced permeability and retention effect of solid tumors: next-generation chemotherapeutics and photodynamic therapy—problems, solutions, and prospects, Microcirculation 23 (3) (2016) 173–182.
[6] M. Li, Z. Tang, D. Zhang, H. Sun, H. Liu, Y. Zhang, Y. Zhang, X. Chen, Doxorubicin-loaded polysaccharide nanoparticles suppress the growth of murine colorectal carcinoma and inhibit the metastasis of murine mammary carcinoma in rodent models, Biomaterials 51 (2015) 161–172.
[7] Z. Tang, C. He, H. Tian, J. Ding, B.S. Hsiao, B. Chu, X. Chen, Polymeric nanostructured materials for biomedical applications, Prog. Polym. Sci. 60 (2016) 86–128.
[8] W. Song, Z. Tang, D. Zhang, X. Wen, S. Lv, Z. Liu, M. Deng, X. Chen, Solid tumor therapy using a cannon and pawn combination strategy, Theranostics 6 (7) (2016) 1023–1030.
[9] J. Wu, C. Tang, C. Yin, Co-delivery of doxorubicin and interleukin-2 via chitosan based nanoparticles for enhanced antitumor efficacy, Acta Biomater. 47 (2017) 81–90.
[10] L. Zhang, Y. Zhang, L. Tai, K. Jiang, C. Xie, Z. Li, Y.-Z. Lin, G. Wei, W. Lu, W. Pan, Functionalized cell nucleus-penetrating peptide combined with doxorubicin for synergistic treatment of glioma, Acta Biomater. 42 (2016) 90–101.
[11] T. Thambi, S. Son, D.S. Lee, J.H. Park, Poly(ethylene glycol)-b-poly(lysine) copolymer bearing nitroaromatics for hypoxia-sensitive drug delivery, Acta Biomater. 29 (2016) 261–270.
[12] L. Qiu, Q. Hu, L. Cheng, L. Li, C. Tian, W. Chen, Q. Chen, W. Hu, L. Xu, J. Yang, L. Cheng, D. Chen, CRGDyK modified pH responsive nanoparticles for specific intracellular delivery of doxorubicin, Acta Biomater. 30 (2016) 285–298.
[13] W. Hu, L. Qiu, L. Cheng, Q. Hu, Y. Liu, Z. Hu, D. Chen, L. Cheng, Redox and pH dual responsive poly(amidoamine) dendrimer-poly (ethylene glycol) conjugates for intracellular delivery of doxorubicin, Acta Biomater. 36 (2016) 241–253.
[14] C.-C. Cheng, F.-C. Chang, W.-Y. Kao, S.-M. Hwang, L.-C. Liao, Y.-J. Chang, M.-C. Liang, J.-K. Chen, D.-J. Lee, Highly efficient drug delivery systems based on functional supramolecular polymers: In vitro evaluation, Acta Biomater. 33 (2016) 194–202.
[15] M. Li, Z. Tang, Y. Zhang, S. Lv, Q. Li, X. Chen, Targeted delivery of cisplatin by LHRH-peptide conjugated dextran nanoparticles suppresses breast cancer growth and metastasis, Acta Biomater. 18 (2015) 132–143.
[16] P. Yu, H. Yu, C. Guo, Z. Cui, X. Chen, Q. Yin, P. Zhang, X. Yang, H. Cui, Y. Li, Reversal of doxorubicin resistance in breast cancer by mitochondria-targeted pH-responsive micelles, Acta Biomater. 14 (2015) 115–124.
[17] H. Maeda, Toward a full understanding of the EPR effect in primary and metastatic tumors as well as issues related to its heterogeneity, Adv. Drug Del. Rev. 91 (2015) 3–6.
[18] Y. Huang, Z. Tang, X. Zhang, H. Yu, H. Sun, X. Pang, X. Chen, PH-triggered charge-reversal polypeptide nanoparticles for cisplatin delivery: preparation and in vitro evaluation, Biomacromolecules 14 (6) (2013) 2023–2032.
[19] T.-M. Sun, Y.-C. Wang, F. Wang, J.-Z. Du, C.-Q. Mao, C.-Y. Sun, R.-Z. Tang, Y. Liu, J. Zhu, Y.-H. Zhu, Cancer stem cell therapy using doxorubicin conjugated to gold nanoparticles via hydrazone bonds, Biomaterials 35 (2) (2014) 836–845.
[20] S. Ruan, M. Yuan, L. Zhang, G. Hu, J. Chen, X. Cun, Q. Zhang, Y. Yang, Q. He, H. Gao, Tumor microenvironment sensitive doxorubicin delivery and release to glioma using angiopep-2 decorated gold nanoparticles, Biomaterials 37 (2015) 425–435.
[21] J.-Z. Du, X.-J. Du, C.-Q. Mao, J. Wang, Tailor-made dual pH-sensitive polymer–doxorubicin nanoparticles for efficient anticancer drug delivery, J. Am. Chem. Soc. 133 (44) (2011) 17560–17563.
[22] K. Wang, X. Zhang, Y. Liu, C. Liu, B. Jiang, Y. Jiang, Tumor penetrability and anti-angiogenesis using iRGD-mediated delivery of doxorubicin-polymer conjugates, Biomaterials 35 (30) (2014) 8735–8747.
[23] Z. Jia, L. Wong, T.P. Davis, V. Bulmus, One-Pot conversion of RAFT-generated multifunctional block copolymers of HPMA to doxorubicin conjugated acid- and reductant-sensitive crosslinked micelles, Biomacromolecules 9 (11) (2008) 3106–3113.
[24] A.M. Mansour, J. Drevs, N. Esser, F.M. Hamada, O.A. Badary, C. Unger, I. Fichtner, F. Kratz, A new approach for the treatment of malignant melanoma: enhanced antitumor efficacy of an albumin-binding doxorubicin prodrug that is cleaved by matrix metalloproteinase 2, Cancer Res. 63 (14) (2003) 4062–4066.
[25] S. Banerjee, K. Todkar, G. Chate, J. Khandare, Prodrug Conjugate Strategies in Targeted Anticancer Drug Delivery Systems, Targeted Drug Delivery: Concepts and Design, Springer, 2015, pp. 367–387.
[26] R.S. DiPaola, J. Rinehart, J. Nemunaitis, S. Ebbinghaus, E. Rubin, T. Capanna, M. Ciardella, S. Doyle-Lindrud, S. Goodwin, M. Fontaine, N. Adams, A. Williams, M. Schwartz, G. Winchell, K. Wickersham, P. Deutsch, S.-L. Yao, Characterization of a novel prostate-specific antigen-activated peptide-doxorubicin conjugate in patients with prostate cancer, J. Clin. Oncol. 20 (7) (2002) 1874–1879.
[27] L. Zhu, T. Wang, F. Perche, A. Taigind, V.P. Torchilin, Enhanced anticancer activity of nanopreparation containing an MMP2-sensitive PEG-drug conjugate and cell-penetrating moiety, Proc. Natl. Acad. Sci. U.S.A. 110 (42) (2013) 17047–17052.
[28] W.-H. Chen, G.-F. Luo, Q. Lei, H.-Z. Jia, S. Hong, Q.-R. Wang, R.-X. Zhuo, X.-Z. Zhang, MMP-2 responsive polymeric micelles for cancer-targeted intracellular drug delivery, Chem. Commun. 51 (3) (2015) 465–468.
[29] S.-I. Ishii, Legumain: asparaginyl endopeptidase, in: J.B. Alan (Ed.), Methods Enzymol., Academic Press, 1994, pp. 604–615.
[30] Y. Morita, H. Araki, T. Sugimoto, K. Takeuchi, T. Yamane, T. Maeda, Y. Yamamoto, K. Nishi, M. Asano, K. Shirahama-Noda, M. Nishimura, T. Uzu, I. Hara-Nishimura, D. Koya, A. Kashiwagi, I. Ohkubo, Legumain/asparaginyl endopeptidase controls extracellular matrix remodeling through the degradation of fibronectin in mouse renal proximal tubular cells, FEBS Lett. 581 (7) (2007) 1417–1424.
[31] K. Shirahama-Noda, A. Yamamoto, K. Sugihara, N. Hashimoto, M. Asano, M. Nishimura, I. Hara-Nishimura, Biosynthetic processing of cathepsins and lysosomal degradation are abolished in asparaginyl endopeptidase-deficient mice, J. Biol. Chem. 278 (35) (2003) 33194–33199.
[32] Z. Liu, M. Xiong, J. Gong, Y. Zhang, N. Bai, Y. Luo, L. Li, Y. Wei, Y. Liu, X. Tan, R. Xiang, Legumain protease-activated TAT-liposome cargo for targeting tumours and their microenvironment, Nat. Commun. 5 (2014).
[33] J.-M. Chen, P.M. Dando, N.D. Rawlings, M.A. Brown, N.E. Young, R.A. Stevens, E. Hewitt, C. Watts, A.J. Barrett, Cloning, isolation, and characterization of mammalian legumain, an asparaginyl endopeptidase, J. Biol. Chem. 272 (12) (1997) 8090–8098.
[34] Y. Lin, C. Wei, Y. Liu, Y. Qiu, C. Liu, F. Guo, Selective ablation of tumor-associated macrophages suppresses metastasis and angiogenesis, Cancer Sci. 104 (9) (2013) 1217–1225.
[35] C. Liu, C. Sun, H. Huang, K. Janda, T. Edgington, Overexpression of legumain in tumors is significant for invasion/metastasis and a candidate enzymatic target for prodrug therapy, Cancer Res. 63 (11) (2003) 2957–2964.
[36] M.H. Haugen, K. Boye, J.M. Nesland, S.J. Pettersen, E.V. Egeland, T. Tamhane, K. Brix, G.M. Maelandsmo, K. Flatmark, High expression of the cysteine proteinase legumain in colorectal cancer – implications for therapeutic targeting, Eur. J. Cancer 51 (1) (2015) 9–17.
[37] J. Gawenda, F. Traub, H.J. Lück, H. Kreipe, R. von Wasielewski, Legumain expression as a prognostic factor in breast cancer patients, Breast Cancer Res. Treat. 102 (1) (2007) 1–6.
[38] L. Wang, S. Chen, M. Zhang, N. Li, Y. Chen, W. Su, Y. Liu, D. Lu, S. Li, Y. Yang, Legumain: a biomarker for diagnosis and prognosis of human ovarian cancer, J. Cell. Biochem. 113 (8) (2012) 2679–2686.
[39] Y. Ohno, J. Nakashima, M. Izumi, M. Ohori, T. Hashimoto, M. Tachibana, Association of legumain expression pattern with prostate cancer invasiveness and aggressiveness, World J. Urol. 31 (2) (2013) 359–364.
[40] A. Sandberg, G. Lindell, B.N. Källström, R.M. Branca, K.G. Danielsson, M. Dahlberg, B. Larson, J. Forshed, J. Lehtiö, Tumor proteomics by multivariate

analysis on individual pathway data for characterization of vulvar cancer phenotypes, Mol. Cell. Proteomics 11 (7) (2012) 112 016998.
[41] R.V. Murthy, G. Arbman, J. Gao, G.D. Roodman, X.-F. Sun, Legumain expression in relation to clinicopathologic and biological variables in colorectal cancer, Clin. Cancer Res. 11 (6) (2005) 2293–2299.
[42] N. Li, Q. Liu, Q. Su, C. Wei, B. Lan, J. Wang, G. Bao, F. Yan, Y. Yu, B. Peng, J. Qiu, X. Yan, S. Zhang, F. Guo, Effects of legumain as a potential prognostic factor on gastric cancers, Med. Oncol. 30 (3) (2013) 1–12.
[43] S. Lin, F. Deng, P. Huang, L. Li, L. Wang, Q. Li, L. Chen, H. Chen, K. Nan, A novel legumain protease-activated micelle cargo enhances anticancer activity and cellular internalization of doxorubicin, J. Mater. Chem. B 3 (29) (2015) 6001–6012.
[44] D. Liao, Z. Liu, W. Wrasidlo, T. Chen, Y. Luo, R. Xiang, R.A. Reisfeld, Synthetic enzyme inhibitor: a novel targeting ligand for nanotherapeutic drug delivery inhibiting tumor growth without systemic toxicity, Nanomed. Nanotechnol. Biol. Med. 7 (6) (2011) 665–673.
[45] K.M. Bajjuri, Y. Liu, C. Liu, S.C. Sinha, The legumain protease-activated auristatin prodrugs suppress tumor growth and metastasis without toxicity, ChemMedChem 6 (1) (2011) 54–59.
[46] Y. Liu, K.M. Bajjuri, C. Liu, S.C. Sinha, Targeting cell surface alpha (v) beta (3) integrin increases therapeutic efficacies of a legumain protease-activated auristatin prodrug, Mol. Pharm. 9 (1) (2011) 168–175.
[47] R.L. Smith, O.A.H. Åstrand, L.M. Nguyen, T. Elvestrand, G. Hagelin, R. Solberg, H.T. Johansen, P. Rongved, Synthesis of a novel legumain-cleavable colchicine prodrug with cell-specific toxicity, Biorg. Med. Chem. 22 (13) (2014) 3309–3315.
[48] L. Stern, R. Perry, P. Ofek, A. Many, D. Shabat, R. Satchi-Fainaro, A novel antitumor prodrug platform designed to be cleaved by the endoprotease legumain, Bioconjugate Chem. 20 (3) (2009) 500–510.
[49] K. Breistøl, H.R. Hendriks, D.P. Berger, S.P. Langdon, H.H. Fiebig, O. Fodstad, The antitumour activity of the prodrug N-L-leucyl-doxorubicin and its parent compound doxorubicin in human tumour xenografts, Eur. J. Cancer 34 (10) (1998) 1602–1606.
[50] W. Song, Z. Tang, D. Zhang, Y. Zhang, H. Yu, M. Li, S. Lv, H. Sun, M. Deng, X. Chen, Anti-tumor efficacy of c(RGDfK)-decorated polypeptide-based micelles co-loaded with docetaxel and cisplatin, Biomaterials 35 (9) (2014) 3005–3014.
[51] W. Song, Z. Tang, M. Li, S. Lv, H. Sun, M. Deng, H. Liu, X. Chen, Polypeptide-based combination of paclitaxel and cisplatin for enhanced chemotherapy efficacy and reduced side-effects, Acta Biomater. 10 (3) (2014) 1392–1402.
[52] W. Song, M. Li, Z. Tang, Q. Li, Y. Yang, H. Liu, T. Duan, H. Hong, X. Chen, Methoxypoly(ethylene glycol)-block-poly(L-glutamic acid)-loaded cisplatin and a combination with iRGD for the treatment of non-small-cell lung cancers, Macromol. Biosci. 12 (11) (2012) 1514–1523.
[53] X. Duan, Y. Li, Physicochemical characteristics of nanoparticles affect circulation, biodistribution, cellular internalization, and trafficking, Small 9 (9–10) (2013) 1521–1532.
[54] S. Lv, M. Li, Z. Tang, W. Song, H. Sun, H. Liu, X. Chen, Doxorubicin-loaded amphiphilic polypeptide-based nanoparticles as an efficient drug delivery system for cancer therapy, Acta Biomater. 9 (12) (2013) 9330–9342.